Journal of Power Sources 196 (2011) 10213–10221

Contents lists available at SciVerse ScienceDirect

Journal of Power Sources

journal homepage: www.elsevier.com/locate/jpowsour

Calendar and PHEV cycle life aging of high-energy, lithium-ion cells containing blended spinel and layered-oxide cathodes

J. Belt [a], V. Utgikar [b], I. Bloom [c,*]

[a] Idaho National Laboratory, 2525N. Fremont, Idaho Falls, ID 83415, United States
[b] University of Idaho, Department of Chemical Engineering, 1776 Science Center Drive, Idaho Falls, ID 83402, United States
[c] Argonne National Laboratory, 9700 S. Cass Avenue, Argonne, IL 60439, United States

ARTICLE INFO

Article history:
Received 23 June 2011
Received in revised form 15 August 2011
Accepted 16 August 2011
Available online 22 August 2011

Keywords:
PHEV battery testing
Performance degradation
Curve-fitting
Calendar life
Charge-sustaining cycling
Charge-depleting cycling

ABSTRACT

One hundred seven commercially available, off-the-shelf, 1.2-Ah cells were tested for calendar life and CS cycle- and CD cycle-life using the new USABC PHEV Battery Test Manual. Here, the effects of temperature on calendar life, on CS cycle life, and on CD cycle life; the effects of SOC on calendar life and on CS cycle life; and the effects of rest time on CD cycle life were investigated. The results indicated that the test procedures caused performance decline in the cells in an expected manner, calendar < CS cycling < CD cycling. In some cases, the kinetic law changed with test type, from linear-with-time to about t^2. Additionally, temperature was found to stress the cells more than SOC, causing increased changes in performance with increasing temperature.

1. Introduction

Lithium-ion batteries continue to attract much interest in applications where high specific or volumetric power or energy is required. High-energy lithium-ion batteries are also being considered for automotive applications by the U.S. Department of Energy-supported U.S. Advanced Battery Consortium (USABC) [1]. The batteries usually consist of a metal-oxide positive electrode, a carbon negative electrode, and an organic electrolyte containing dissolved lithium salts.

Layered-oxide cathodes, such as $Li(Ni_{1/3}Mn_{1/3}Co_{1/3})O_2$, represent good candidates for automotive applications because of their high specific capacity [2]. However, the cycle life of this oxide was not as high as desired [3]. On the other hand, spinel oxides, such as $LiMn_2O_4$, are also viable candidates. These oxides are low-cost and have fast kinetics, which makes the oxide suitable for high-power applications [2]. The spinels were reported to have lower specific capacity than the layered oxides [2] and to degrade rapidly due to manganese dissolution [3–6]. There have been reports in the literature that blending these two materials produced a composite with the benefits of both [7–12].

Two U.S. Department of Energy national laboratories, Argonne National Laboratory (ANL) and Idaho National Laboratory (INL), continue to collaborate to understand the causes of performance decline in lithium-ion batteries. Results from this collaboration using three positive electrode materials—$LiNi_{0.8}Co_{0.2}O_2$, $LiNi_{0.8}Co_{0.1}Al_{0.1}O_2$, and $Li_{1.05}(Mn_{1/3}Co_{1/3}Ni_{1/3})_{0.95}O_2$—are given in Refs. [13–18].

The procedures outlined in the USABC test manuals [19–21] are intended to show the promise of a technology versus a set of performance and cost targets. No knowledge of the actual battery chemistry is needed. Thus, the evaluation of cells concentrates on their performance and life and how their life is affected by SOC, time, temperature and type of test. Calendar and cycle life tests were performed to determine the aging characteristics of the blended cathode material under plug-in hybrid electric vehicle (PHEV) testing conditions [19]. It should be noted that the calendar tests in the PHEV and hybrid-electric vehicle (HEV) [20] manuals are essentially the same. The cycle life test is more complex, depending on what is to be learned. Instead of just one cycling mode of operation, charge-sustaining, as in an HEV, the PHEV operates in charge-depleting (CD) as well as charge-sustaining (CS) modes, as shown schematically in Fig. 1. In the CD mode of operation, the battery powers the vehicle directly; the internal-combustion engine is not used at all. After a while, the battery energy becomes exhausted. At this low state of charge, the PHEV will operate in CS mode, similar to that of a hybrid-electric vehicle.

* Corresponding author. Tel.: +1 630 252 4516; fax: +1 630 252 4176.
E-mail address: ira.bloom@anl.gov (I. Bloom).

0378-7753/$ – see front matter © 2011 Elsevier B.V. All rights reserved.
doi:10.1016/j.jpowsour.2011.08.067

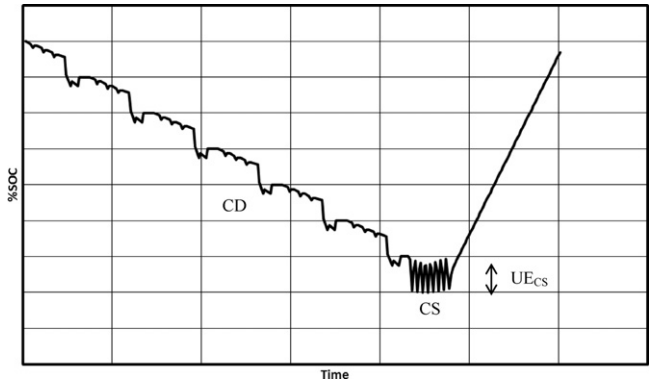

Fig. 1. Schematic showing the two PHEV operating modes, charge-depleting and charge-sustaining (after Ref. [19]). In charge-depleting mode, the internal-combustion engine is not used; energy from the battery alone powers the vehicle. The charge-sustaining mode is similar to that of the HEV; the power from the battery supplements that from the engine. The abbreviation, UE_{CS}, shown in the figure, is the SOC window from which the usable energy in CS mode is based.

The PHEV-related test methods and protocols are new and have not been validated. The objective of work below, in part, is to validate that the test methods stress the battery as expected. In the study described below, the effects of temperature on calendar life, on CS cycle life, and on CD cycle life; the effects of SOC on calendar life and on CS cycle life; and the effects of rest time on CD cycle life were investigated using commercially-available, 18650-size cells. The results of this work will help elucidate the additional stresses on the battery when it is cycled.

2. Experimental method

2.1. Testing

One hundred-seven commercially-available, off-the-shelf, 1.2-Ah, 18650-size cells were used in this work. These cells contained a physically-blended Li–Ni–Mn–Co layered-oxide and Li–Mn–O spinel cathode, an organic electrolyte, and a carbon anode. The test matrix is presented in Table 1. All cells were charged using the manufacturer's recommended algorithm: charge at 1.2 A to 4.2 V, followed by a potentiostatic hold at 4.2 V for a total charge time of 2 h or until the current drops below 50 mA.

Before the start of the aging tests, all cells were characterized in terms of their 10-kW rate capacities and by the hybrid-pulse power characterization (HPPC) test at 30 °C. The cell groups were aged as shown in Table 1 and the performance was averaged for each group. The cells tested at temperatures higher than 30 °C were heated to the test temperature and allowed to equilibrate for 8 h before the aging period began. Every 32 days, testing was stopped and the cells were allowed to rest at 30 °C for at least 8 h. Changes in cell performance were measured by repeating the characterization tests at 30 °C (a reference performance test, or RPT). Testing was then resumed for a total of 10 RPTs.

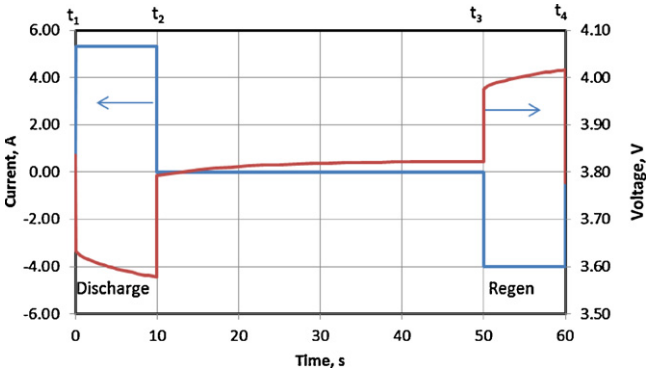

Fig. 2. HPPC profile and voltage response for a typical cell.

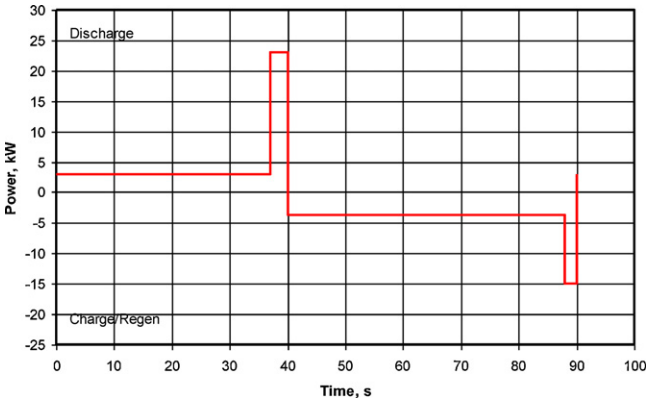

Fig. 3. Charge-sustaining cycling profile [19]. The power levels given on the vertical axis are divided by the BSF to yield the actual power levels used to test a given battery. The unscaled profile removes 50 Wh during the discharge portion of the cycle; the regen portion charges the battery with 46.2 Wh of energy, producing a net removal of 3.8 Wh.

The HPPC test was a constant-current test and consisted of removing 10% of the rated capacity at the C/1 rate, resting for 1-h and applying the test profile. This test sequence was repeated for a total of 9 profiles. Fig. 2 shows the HPPC test profile and the voltage response of a typical cell. For the cells tested, the discharge current in the HPPC profile was 5.3 A, and the regeneration (regen) current, 4.0 A.

Based on the initial HPPC results, the average, calculated battery-size factor (BSF) was 1400 cells. The BSF was used to scale the CS and CD cycle profiles to accommodate the capabilities of the test cells. The generic CS and CD cycle profiles [19] are given in Figs. 3 and 4, respectively. In this experiment, all SOCs for aging were defined in terms of cell potentials: 3.69, 3.89, and 4.09 V for 30, 60, and 90% SOC, respectively. For CS cycling, the battery was discharged to the target SOC at the *C*/1 rate and allowed to rest for

Table 1
Test matrix used in this work. Each entry in the table represents the number of cells tested under that condition.

Test	Temperature, °C				SOC		Rest time, min		
	30	40	50	60	30	90	0	20	40
Calendar life (60% SOC)	10	5	5	4					
Calendar life (30 °C)					5	5			
CS cycle life (60% SOC)	9	5	5	5					
CS cycle life (30 °C)					5	5			
CD cycle life (15-min rest time)	9	5	5	5					
CD cycle life (30 °C)							5	5	5

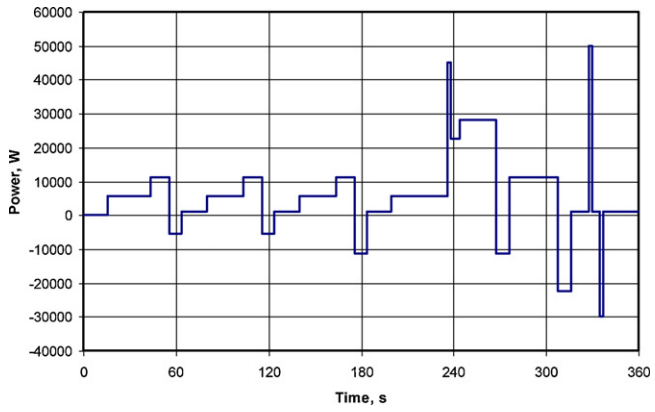

Fig. 4. Charge-depleting cycling profile [19]. The power levels given on the vertical axis are divided by the BSF to yield the actual power levels used to test a given battery. The unscaled profile removes 545.61 Wh of energy; about 6.2 repetitions of the profile remove 3.4 kWh.

1 h. The CS profile was repeated continuously for 32 days at the test temperature.

Starting from the initial state of charge (~90% SOC, the PHEV charge target), the CD cycling profile was repeated continuously until the BSF-scaled, 3.4 kWh of energy had been removed. The cell was then recharged to ~90% SOC and allowed to rest for the times indicated in Table 1. The discharge–rest–recharge process was repeated continuously for 32 days at the test temperature, at which time an HPPC test was performed to re-characterize the cell and to gauge capacity fade and resistance rise.

The data from the HPPC test were used to calculate resistance vs. voltage curves. The discharge and regen resistances (R_d and R_r, respectively) were calculated using the equations shown in Eq. (1). For R_d, V_{t1} and I_{t1} (see Fig. 2 for definitions of t_1 and t_2) are the voltage and current, respectively, right before the discharge pulse, and V_{t2} and I_{t2} are the voltage and current 10 s later. For R_r, V_{t3}, I_{t3}, V_{t4} and I_{t4} (see Fig. 2 for definitions of t_3 and t_4) follow analogously.

$$R_d = \frac{V_{t_1} - V_{t_2}}{I_{t_1} - V_{t_2}}; \quad R_r = \frac{V_{t_3} - V_{t_4}}{I_{t_3} - V_{t_4}} \tag{1}$$

An example plot is shown in Fig. 5 for a typical cell. As the cell aged, the discharge and regen resistances, generally, increased with time.

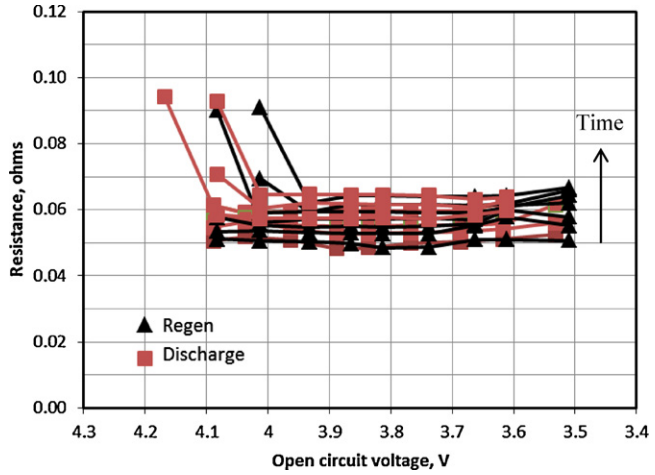

Fig. 5. Discharge and regen resistance vs. open circuit voltage with time for a typical cell.

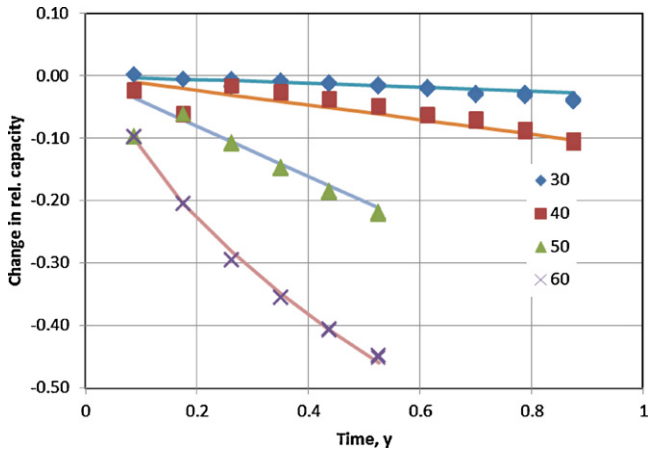

Fig. 6. The change in relative cell capacity vs. time for the calendar life cells. The values in the legend are aging temperature in °C; the negative values indicate capacity loss. The cells at 30, 40, and 50 °C tended to follow a different capacity loss mechanism than those at 60 °C. The data are shown as markers, and the fit, as a solid curve.

2.2. Data reduction

The cell capacity and resistance at 60% SOC were collected and normalized to $t = 0$ before curve fitting. Normalizing the data from each cell to that point minimized the effects of cell-to-cell variation and emphasized the relative change in the data from each cell.

For most of the work described below, the change in the relative data from each test condition was fit using the LINEST function in Microsoft® EXCEL or using the non-linear regression function in Systat® SigmaPlot®. In some cases, such as in CS cycling experiment that used SOC as the experimental parameter (see Section 3.2.2), the change in the normalized data was fit using Battery Life Estimation (BLE) software [22].

Briefly, the BLE software is based on the mathematics and reasoning given in Ref. [23a]. The BLE software fits a proposed degradation model to experimental data using robust linear and non-linear regression techniques. The software incorporates a simple error model that attempts to quantify the level of deviations between the data and the degradation model. It also uses the fitted model to estimate battery life (Monte Carlo techniques). The non-linear regression uses the Levenberg–Marquardt technique [23b]. In each type of regression, each point is analyzed and iteratively re-weighted using the biweight transformation [23c]. The biweight transformation is most commonly applied to the residuals from a linear or non-linear fit. The biweight transformation has the advantage that it allows the analyst to carry out subsequent weighted linear or non-linear fits that are robust and resistive to outliers in the data [23c].

3. Results

3.1. Calendar life cells

3.1.1. Effect of temperature (60% SOC)

Capacity. The change in the relative capacity of the cells versus time is shown in Fig. 6. From the figure, there were two processes occurring. One capacity fade mechanism, in the temperature range of 30–50 °C, followed linear-with-time kinetics, and the other, at 60 °C, followed parabolic ($t^{1/2}$) kinetics.

From the fit using $\Delta(Rel.\ capacity) = -\exp(A + B/T)t$, where A and B are constants, t is calendar time, and T is absolute temperature, the data from the 30, 40, and 50 °C tests also followed Arrhenius-like kinetics. The fitting parameters and the standard errors (s.e.) for this group of data were $A = 3.84 \times 10^1$ (s.e. $= 4.86 \times 10^{-1}$),

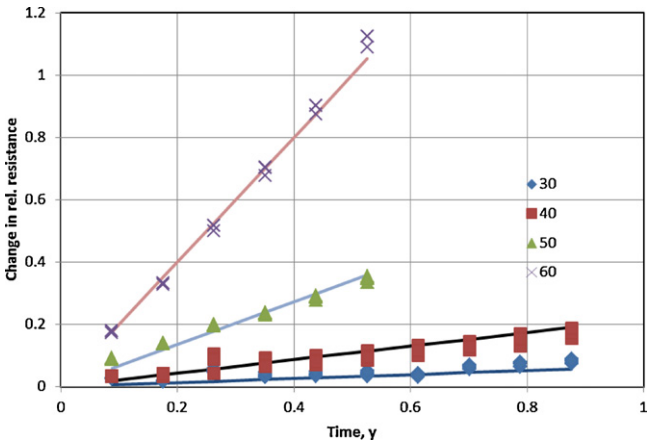

Fig. 7. Change in relative resistance vs. time for the calendar life cells. The data are shown as markers, and the fit, as a solid curve.

$B = -1.269 \times 10^4$ (1.55×10^2) K, and $r^2 = 0.97$. From the high value of r^2, the fit was very good. The value of E_a, the activation energy calculated from the value of B, for this degradation process was 105.50 kJ mol^{-1}.

The data from the 60 °C were fit to the equation, $\Delta(\textit{Rel. capacity}) = at^{1/2} + c$, where a and c are fitting constants. From the fit, the values of a, c, and r^2 were -8.33×10^{-1} $(8.65 \times 10^{-3})y^{-1/2}$, -1.44×10^{-1} (4.54×10^{-3}), and 0.99, respectively. Again, the high value of r^2 indicated that the fit was very good. The nonzero value of c reflects the error in the average capacity measurement.

Resistance. The values of cell resistance at 60% SOC were treated as described above. A plot of the change in the relative values is given in Fig. 7. From the plot, all data sets seemed to follow linear-with-time kinetic laws.

The values of A and B from the least-squares fitting were 3.54×10^1 (2.97×10^{-1}) and -1.26×10^4 (9.97×10^1) K and the value of r^2 was 0.99, indicating that the fit was excellent. The estimated value of E_a was 96.10 kJ mol^{-1} for this degradation process.

3.1.2. Effect of SOC (30 °C)

Capacity. The effect of cell SOC on cell capacity is shown in Fig. 8, along with the least-squares fit to the data. From the figure, capacity decreases with time at all SOCs. Using the linear-with-time kinetic expression, $At + B$, the data were fit to this equation with values of r^2 of 0.99 or better. The values of the least-squares fitting parameters, along the standard error, for these curves are given in Table 2

Table 2
Fitting parameters from the calendar life SOC cells.

%SOC	A (s.e.), y^{-1}	B (s.e.)
30	-3.40×10^{-2} (9.62×10^{-4})	1.82×10^{-2} (4.74×10^{-4})
60	-4.59×10^{-2} (9.55×10^{-4})	1.49×10^{-2} (4.71×10^{-4})
90	-8.74×10^{-2} (2.32×10^{-3})	1.32×10^{-2} (1.14×10^{-4})

From the data in Table 2, the values A seem to correlate with SOC. Indeed, the correlation coefficient between the values of SOC and the values of A was −0.95, indicating that the rate of capacity decline increased with increasing SOC.

Resistance. The effects of SOC and time on the resistance of the cells are shown in Fig. 9. It can be seen from the figure that the effect of SOC on cell resistance was not simple. At 30% SOC, the resistance of the cells, effectively, did not change during the course of the experiment; on the other hand, the resistances of the cells at 60 and 90% SOC did change. In the 60 and 90% SOC data, the resistance did not change significantly during the time interval of 0.17 to 0.53y. After that point the resistance in these cells tended to increase.

3.2. CS cycle life

3.2.1. Effect of temperature (60% SOC)

Capacity. The data from the cycling-at-temperature experiment are shown in Fig. 10a, along with fits to the data. The data could not be fit to an Arrhenius-like expression; there were excessive errors in the resulting fit, most likely from the fewer number of observations at 50 °C. Fewer observations at the high temperature would skew the fitting because of the uneven weight given to the observations that are present in the lower-temperature studies. Consequently, the data were fit as four independent curves to the general equation, $At^{1/2} + B$, indicating parabolic kinetics. The values of the fitting parameters and r^2 are given in Table 3

An estimate of the activation energy, E_a, for this degradation process was calculated from the values of A in Table 3. From the slope of the line of $\ln(|A|)$ vs. $1/T$, the estimate of E_a was 64.80 kJ mol^{-1} ($r^2 = 0.99$).

Comparing these results to those found in the calendar life test shows the effects that CS cycling imposed on the cells (see Fig. 10b). In all cases, CS cycling increased capacity fade and, in most cases, CS cycling changed the kinetic behaviors. Capacity fade in the calendar life test tended to follow Arrhenius-like, linear-with-time kinetics in the temperature range of 30–50 °C; those from the CS

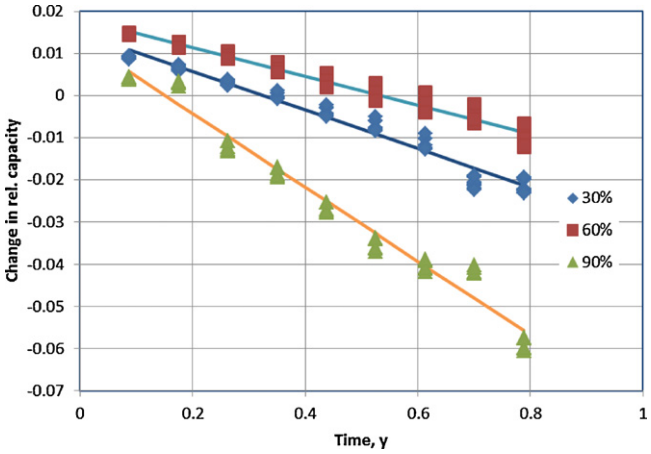

Fig. 8. Change in relative cell capacity vs. time and SOC for the calendar life cells. The data are represented as markers on the plot, and the least-squares fit, as solid curves. The numbers in the legend represent the SOCs used in the experiment.

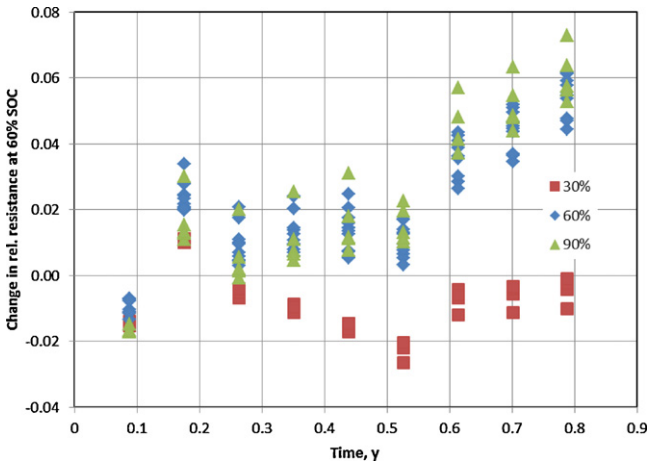

Fig. 9. Change in relative cell resistance vs. time and SOC for the calendar life cells. The numbers in the legend represent the SOCs used in the experiment.

Table 3
Values of the fitting parameters and r^2 from the CS cycling at temperature tests.

Temperature, °C	A, $y^{-1/2}$ (s.e.)	B (s.e.)	r^2
30	-8.23×10^{-2} (2.55×10^{-3})	2.37×10^{-2} (1.68×10^{-3})	0.93
40	-2.10×10^{-1} (2.96×10^{-3})	5.65×10^{-2} (1.94×10^{-3})	0.99
50	-4.80×10^{-1} (2.63×10^{-2})	8.48×10^{-2} (1.57×10^{-2})	0.94
60	-8.15×10^{-1} (1.33×10^{-2})	9.07×10^{-2} (6.23×10^{-3})	0.99

cycle test exhibited $t^{1/2}$ kinetics. Only at 60 °C in the calendar test were parabolic kinetics observed.

Additionally, cycling increased the average fade rates. At 40 °C, the increase was modest from ~10% to ~12% in ~0.88y. The increase was more noticeable at 60 °C, from 35% to 40% in ~0.35y. Clearly, from these results, the majority of the capacity loss was due to the time at elevated temperatures; CS cycling had a relatively minor influence in the capacity loss process.

Resistance. The changes in the relative resistances from the cycling-at-temperature test are shown in Fig. 11, along with fits to these data. These data were fit to the equation, $\Delta(Rel.\ resistance) = \exp(A + B/T)t$, where T is absolute temperature and t is time. The values for A and B were 33.72 (0.84) and −11047.04 K (277.14), respectively. From the value of r^2, 0.99, the fit was very good. The calculated curves using the fitted parameters are also shown in Fig. 11. From the value of B, the estimated value of E_a was 91.84 kJ mol^{-1} for this process.

Comparing these fitting results with those obtained from the calendar life test (see Fig. 12) shows that most of the resistance increases are due to calendar-life effects at all temperatures. At 30 and 40 °C, there were no significant differences between the calendar and CS cycle curves. Only at 50 and 60 °C were significant differences observed; the cells from the CS cycle test displayed about 9–19% additional resistance increase.

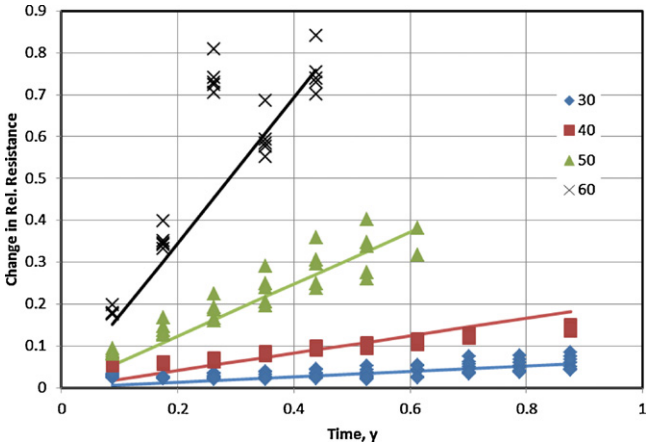

Fig. 11. Effect of temperature on the change in relative resistance vs. time. The numbers in the legend indicate the temperature in °C. Higher temperatures accelerated resistance increase. The observations at about 0.78y from the 40 °C test were missing from the data.

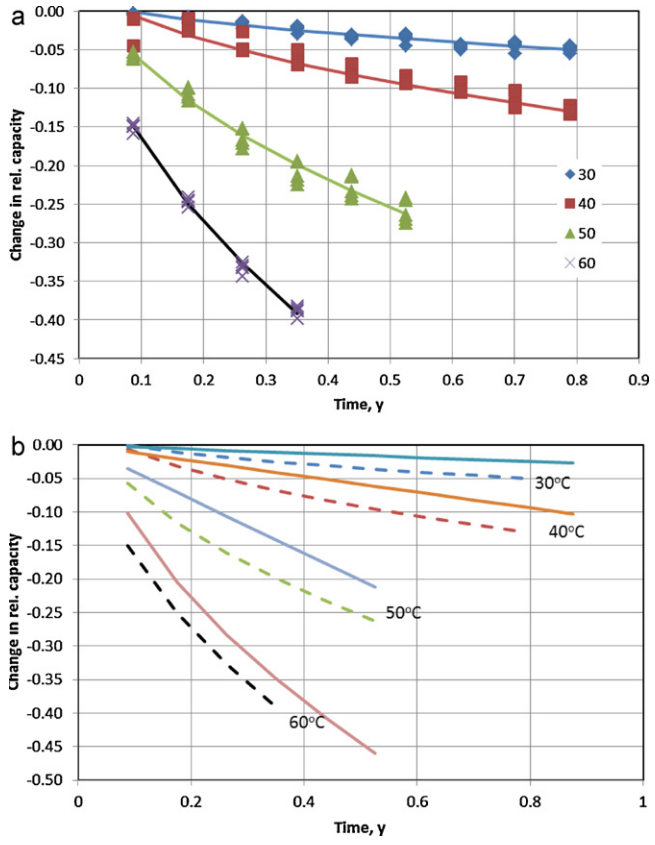

Fig. 10. (a) Effect of temperature of CS cycling on the change in relative capacity vs. time. The numbers in the legend indicate the temperature in °C. Higher temperatures accelerated capacity loss. (b) Change in relative capacity vs. time showing the difference in the fitted curves from the calendar- and CS cycle-life tests. CS cycling increase capacity fade and can change the kinetic behavior of the cells. The solid lines represent the fitted curves from the calendar-life test and the dashed, those from CS cycling.

3.2.2. *Effect of SOC (30 °C)*

Capacity. The changes in relative capacity vs. time data for cells cycled at 30, 60, and 90% SOC are given in Fig. 13, along with the least-squares fit to the data. Here, the change in relative capacity was fit to the equation, $a + b \times SOC \times t$, where a and b are fitting constants, SOC is the state of charge expressed as a decimal fraction and t is time. From the robust regression, the values of a and b were 1.49×10^{-2} (8.01×10^{-6}) and -9.83×10^{-2} SOC^{-1} y^{-1}, respectively. Due to the high cell-to-cell variability (~11%), the

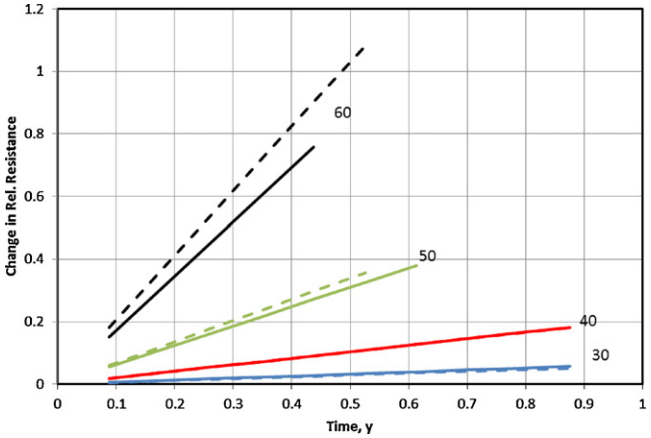

Fig. 12. Change in relative resistance vs. time comparing the fitting results from the calendar and CS-cycling tests. The numbers next to each set of lines represent the test temperature. The lines from the calendar test are shown in solid lines and those from the CS cycle test, as dashed lines.

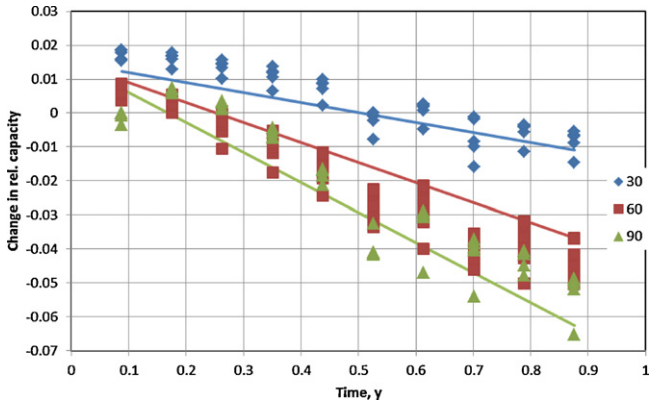

Fig. 13. Effect of SOC on the change in relative capacity vs. time. The numbers in the legend indicate the SOC. The markers represent the data points and the solid lines, the fitted curves. Higher SOCs tended to accelerate capacity loss.

value of r^2 was low, 0.86. The results of this experiment are consistent with those described in the calendar life tests using SOC as the experimental variable, that rate of capacity fade increased with increasing SOC.

Resistance. The effect of SOC and cycling on the relative resistance of the cells is shown in Fig. 14, along with fits to the data. As shown in Fig. 14, the change in relative cell resistance was complex. At 60 and 90% SOC, during the time interval of 0 to ~0.44*y*, the resistance of the cell decreased. After ~0.5*y*, it increased. However, the data from the 30% SOC cells shows that resistance was still decreasing during the time of the test. These observations imply that there was a voltage-driven point where the aging process fundamentally changed.

It is interesting to note that, once the cell was operated above a certain voltage, the inflection point in the resistance vs. time data did not change. That is, the inflection point from the 60 to 90% SOC cells was at the same point in time, ~0.44*y*. Beyond the inflection point, the trends in the data appear to be the same. That is, there was little difference in the trend in the data at 60 and 90% SOC.

3.3. CD cycle life

3.3.1. Effect of temperature

Capacity. The change in relative capacity from this experiment is given in Fig. 15a. From the figure, the effects of two capacity-consuming processes are seen. Indeed, comparing Figs. 6 and 15a shows that they appear to be similar. Both display the effect of

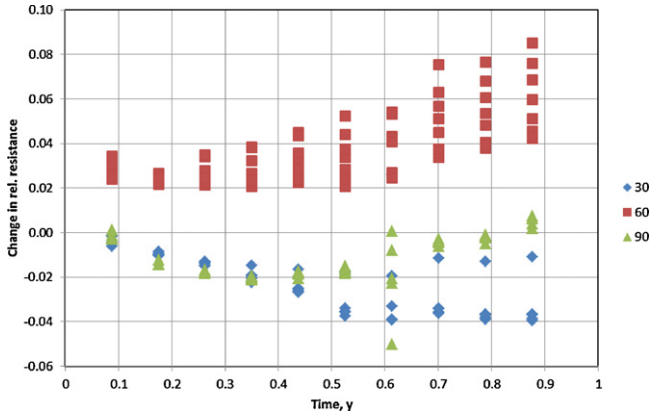

Fig. 14. Effect of SOC on the change in relative resistance at 60% SOC vs. time. The numbers in the legend indicate the SOC. All cells exhibited an interval where resistance decreased. This interval was long at low SOC and relatively short at higher SOC values.

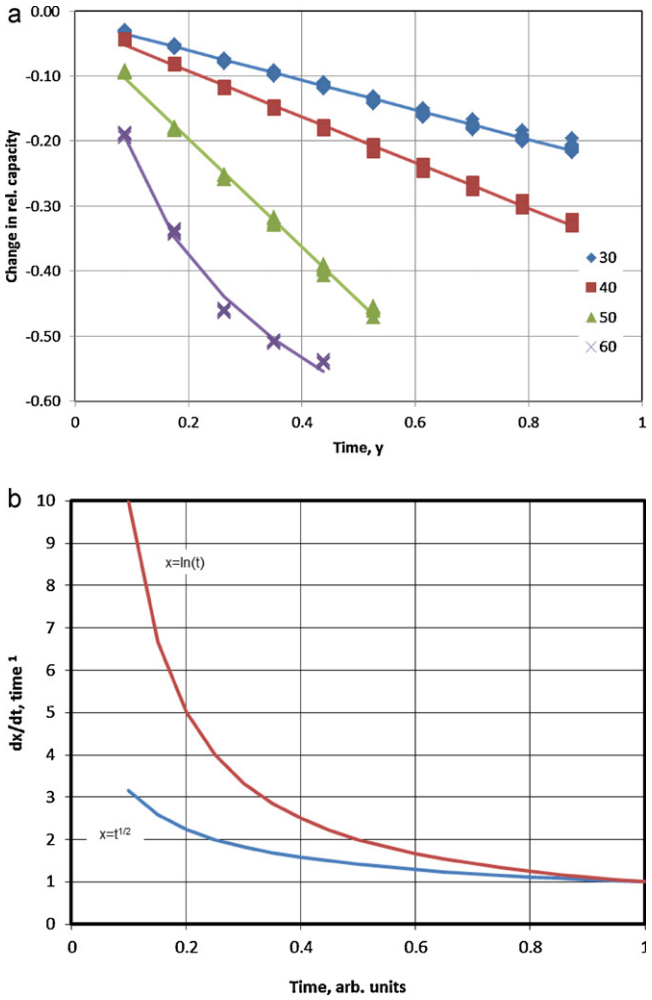

Fig. 15. (a) Change in rel. capacity vs. time for the CD cycle life test. The data are indicated as markers, and the fits, as solid curves. The 30–50 °C cells follow one mechanism, and those at 60 °C, another. (b) Rates of change for two kinetic expressions, $x = t^{1/2}$ and $x = \ln t$. Initially, $d(\ln t)/dt > d(t^{1/2})/dt$.

linear-with-time processes in the temperature range of 30–50 °C and a nonlinear process at 60 °C. As described above in Section 3.2.1, the data could not be fit to an Arrhenius-like expression; there were excessive errors in the resulting fit, most likely from the fewer number of observations at 50 °C. Fewer observations at the high temperature would skew the fitting because of the uneven weight given to the observations that are present at longer times. Fitting the 30–50 °C data to $\Delta(Rel.\ capacity) = at + b$ yielded the values for a, b and r^2 shown in Table 4. Based on the high values of r^2, these fits were very good

At first look, fitting the 60 °C data indicated that equations similar those used by Broussely et al. [24] were directly applicable. That is, dx/dt was proportional to $1/x$, where x is the concentration of lithium (i.e., cell capacity). Fitting the data using the general equation, $t = k_1x^2 + k_2x$, yielded a reasonable value of r^2 of 0.93. However, the high initial rate of change shown in the data was not truly represented. The data were better described by using a mechanistically related, $\ln t$ expression. Both $t^{1/2}$ and $\ln t$ can be used to describe diffusion-limited processes [25,26], but those that depend on $\ln t$ tend to change faster (dx/dt) initially (see Fig. 15b). Fitting the data to the expression given in Eq. (3) yielded the following parameters: $D = -2.25 \times 10^{-1}$ (4.77×10^{-3}) and $E = -7.40 \times 10^{-1}$ (7.54×10^{-3}). The value of r^2 now increased to 0.99.

$$\Delta(Rel.capacity) = D \ln t + E \tag{3}$$

Table 4
Fitting results from the effect of temperature during CD cycling on relative capacity test.

Temperature, °C	a, y^{-1} (s.e.)	b (s.e.)	r^2
30	-2.28×10^{-1} (1.81×10^{-3})	-1.49×10^{-2} (9.84×10^{-4})	0.99
40	-3.52×10^{-1} (3.08×10^{-3})	-2.15×10^{-2} (1.67×10^{-3})	0.99
50	-8.30×10^{-1} (9.54×10^{-3})	-3.05×10^{-2} (3.26×10^{-3})	0.99

The curves in Figs. 6 and 15a show the net effect of CD cycling on the cells. The addition of cycling increased the total capacity fade of the cells as well as the average rate of fade. For example, adding cycling increases the total degradation by about a factor of 2 in ~0.53y at 50 °C, from about 22% to about 45%. The effect of cycling on the 60 °C cells can also be seen, but the net effect is not as great. Here, the increased loss was from 40% to about 55% in 0.43y, along with a change in the fade mechanism.

Resistance. The resistance data from the CD cycling at temperature tests and the fits to these data are given in Fig. 16. An inspection of the data in Fig. 16 shows that three different mechanisms are present. At 30 °C, the rate of change increased with time; at 40 and 50 °C, it remained constant; and at 60 °C, it tended to slow with time.

No simple kinetic expression was found to fit the data shown in Fig. 16; these data were fit independently to three equations. The data from the 30 °C cells was fit by the equation of the form, $At^z + C$. The fitting parameters for this equation were 0.71 (0.02)$y^{-3/2}$, 1.52 (0.10), 3.80×10^{-3} (1.19×10^{-3}), and 0.99 for A, z, C, and r^2, respectively. Even though there were only two data sets, an Arrhenius expression (see capacity fade in this section for form of the equation) was used to fit the data from the 40 and 50 °C cells. The fitting parameters here were 12.00 (0.69), 3829.08 (219.30), and 0.99 for A, B, and r^2, respectively. From the value of B, the estimated value of E_a was 31.8 kJ mol^{-1}. Finally, the data from the 60 °C cell test was fit using a parabolic rate law, $At^{1/2} + C$. The values of the fitting parameters were 1.13 (0.06)$y^{-1/2}$, −0.12 (0.03), and 0.99 for A, C, and r^2, respectively.

Comparing Figs. 7 and 16 shows the effect of CD cycling on resistance increase. At 30 °C, the mechanism changes from linear to non-linear and the average resistance changes from an increase of ~10% to ~50% in 0.79y. It is interesting to note that, at 60 °C, along with the mechanism change, the average rate of resistance increase actually decreased from ~110% to ~64% in 0.43y.

3.3.2. *Effect of rest time (30 °C)*

Capacity. The change in relative capacity of the cell with elapsed time and rest time is shown, along with a fit to the data, in Fig. 17.

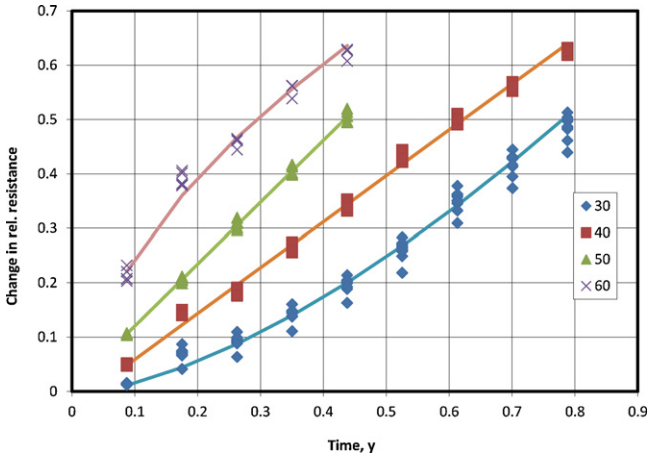

Fig. 16. Change in relative resistance vs. time. The numbers in the legend represent the test temperatures. The data are indicated as markers, and the fits, as curves.

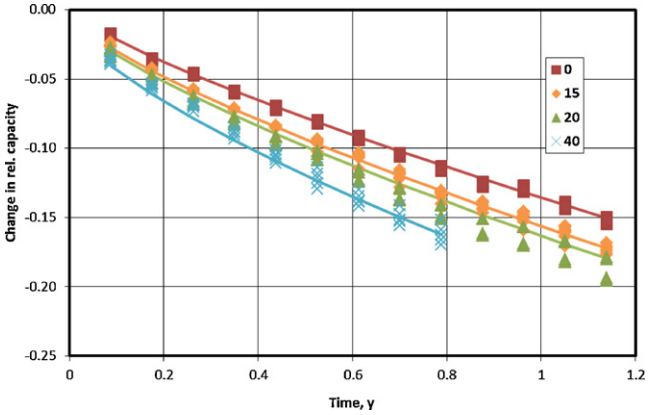

Fig. 17. Change in relative capacity vs. time. The values in the legend indicate the rest time between charge and discharge half-cycles in minutes. The data are shown as markers, and the fit using the best set of parameters, as the solid curves.

Fig. 17 shows that, with no rest time, the degradation rate was the lowest. With longer rest times, the degradation rate increased. The data were fit using $\Delta Q = Ct^z + Dt\rho$, where ΔQ is the change in the relative parameter of interest, such as capacity or cell resistance, t is calendar time, ρ is rest time expressed in calendar years, and C, z, and D are fitting constants. The fitting constants, C, z, and D, were −0.13 (1.80×10^{-3}), 0.71 (1.87×10^{-2}), and −941.42 (51.74), respectively. The high value of r^2, 0.99, indicated that the fit was very good.

The effect of CD cycling on capacity decline can be seen by comparing the fitted curves from the calendar life test and Fig. 17; this comparison is shown in Fig. 18. As expected, capacity loss and the average rate of capacity loss were greater in the cycling test than those from the calendar test. From Fig. 18, the capacity loss in the 0-min-rest-time CD cycling test was about 9.3% in ~0.8y, while that from in the 30 °C calendar test was about 3% in the same amount of time. The 3-fold increase in capacity fade reflects the additional stress caused by CD cycling.

The relative magnitudes of C and D indicate the influences that elapsed time and rest time have on capacity fade. In the cycling

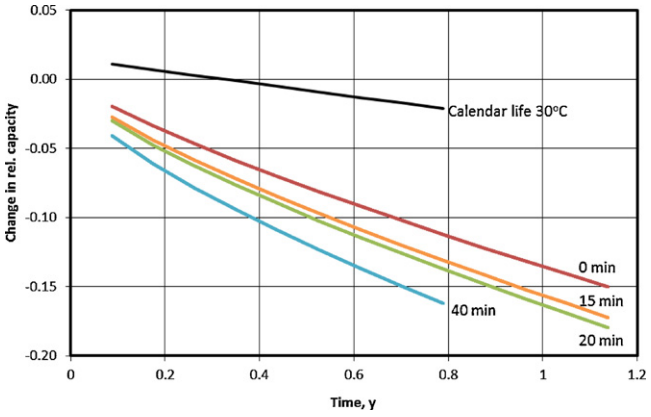

Fig. 18. Fitted curves from Fig. 17 and the calendar data for cells tested at 30 °C, showing the comparison of calendar aging with that from CD cycling. As expected, CD cycling greatly increased the rate of capacity loss.

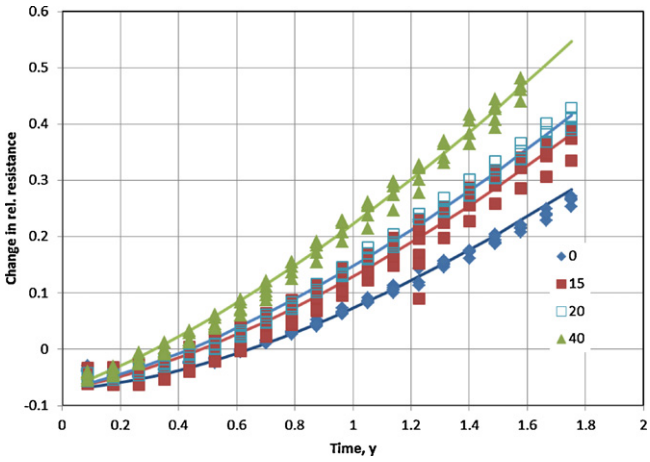

Fig. 19. Change in relative resistance vs. calendar time. The values in the legend reflect the rest time in minutes. The data are shown as markers, and the fit, as a solid curve.

experiment, it appears that there is a strong interaction between the total amount of rest time between charge and discharge and the duration of the test. As shown in Fig. 9, capacity fade is strongly influenced by time at high SOC. With increasing rest time, the cells spend more time idle at high voltage (90% SOC), where degradation would be expected to be faster.

In the calendar test discussed above, capacity fade at 30 °C was proportional to t. With CD cycling, the mechanism became proportional to $t^{0.71}$.

Resistance. The change in the relative cell resistance, along with fits of these data, is shown in Fig. 19. From the figure, the change in cell resistance increases geometrically with elapsed time and is directly proportional to rest time. The data were fit using $\Delta R = Ct^z + Dt\rho + E$, where ΔR is the change in the relative resistance, t is calendar time, ρ is rest time expressed in calendar years, and C, z, D and E are fitting constants

The fit of these data using the same equation used in the capacity fade discussion in Section 3.3.2 further amplifies these observations; the values of the fitting parameters, C, z, D, E and r^2 are 1.43×10^{-1} (3.10×10^{-3}), 1.62 (3.30×10^{-2}), 1.97×10^{4} (3.32×10^{1}), and 0.99, respectively.

Fig. 20 compares this fit to that from the calendar life data at 30 °C. Again, cycling increased the change in cell resistance as well as the average rate of change. For example, the resistance of the cells with no rest time increased 10.5% in ~0.8y; while, in the 30 °C calendar life test, it increased only about 5.7% in the same amount of time. The ~2-fold increase in resistance reflects the additional changes caused by CD cycling.

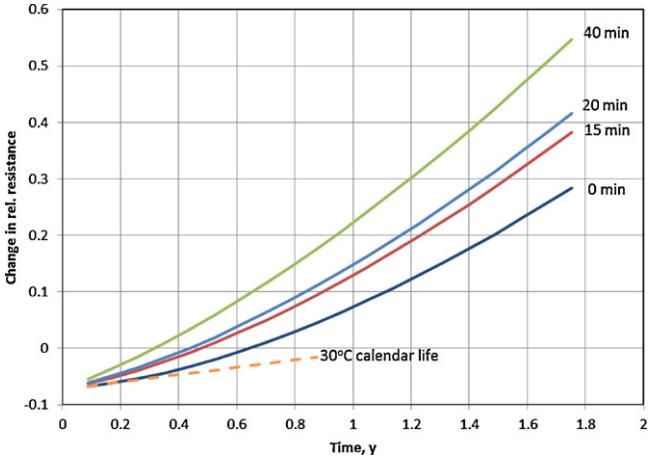

Fig. 20. Comparison of the fitted curves from the rest-time tests and that from the 30 °C calendar life test. The curve representing the 30 °C calendar life fit has been artificially translated 0.073 units down to make the comparison between the curves easier.

As discussed above, the relative magnitudes of the fitting constants, C and D, indicate the influence that calendar time and rest time have on resistance change. In the cycling experiment, it appears that there is a strong interaction between the total amount of rest time between charge and discharge and the duration of the test.

4. Discussion

The capacity fade and resistance increase results from the calendar life test in the temperature range of 30–50 °C and 60% SOC appeared to follow Arrhenius-like kinetics. Similarly, resistance increase seemed to follow Arrhenius-like kinetics. Thus, capacity fade and resistance increase may be caused by thermally-activated processes which were linear with time.

It was interesting to note that resistance increase followed two processes in this test, one that was active in the temperature range of 30–50 °C, and the other, at 60 °C. The rate of resistance increase at 60 °C did not depend on t; instead it depended on $t^{1/2}$. At this temperature, resistance increase may be due to the growth of a solid electrolyte interface layer (SEI), the growth of which can be proportional to $t^{1/2}$ [13,27,28].

Increasing or decreasing the SOC also had effects on the rates of capacity fade and resistance increase. The rate of capacity fade tended to increase with increasing SOC. That is, time at high voltage was deleterious to capacity retention. On the other hand, the changes in resistance were not as simple; cell resistance, effectively, did not change at 30% SOC. At 60% and 90% SOC, cell resistance did increase, but there was no significant difference in its behavior with time at these SOCs. This observation implies that, above 30% SOC, the rate of resistance increase was not sensitive to SOC (or cell voltage).

The results from CS cycling showed that the rates of performance change were very similar to those observed in the calendar life experiment. On the other hand, the results from the CD cycling test were not. There were dramatic changes in the mechanism(s) and rates of performance change in the CD cycling test. Since the amount of energy removed during CD cycling differs from that during CS cycling by about two orders of magnitude, (from Figs. 3 and 4, 3.8 and 545.61 Wh per profile, respectively), the rates of performance change shown above in CS and CD cycling may be linked to energy removal or the wider voltage range used during CD cycling.

5. Conclusions

One hundred-seven commercially-available, off-the-shelf, 1.2-Ah cells were tested for calendar life and CS cycle- and CD cycle-life using the new USABC PHEV Battery Test Manual. Here, the effects of temperature on calendar life, on CS cycle life, and on CD cycle life; the effects of SOC on calendar life and on CS cycle life; and the effects of rest time on CD cycle life were investigated. The results indicated that the test procedures caused performance decline in the cells in an expected manner, calendar < CS cycling < CD cycling. In some cases, the kinetic law changed with test type, from linear-with-time to about t^2. Additionally, temperature was found to stress the cells more than SOC, causing increased changes in performance with increasing temperature.

For maximum cell life, the rest time during CD cycling should be minimal. This may directly impact the design of test profiles.

Acknowledgments

The authors acknowledge many fruitful conversations with Dr. Edward V. Thomas (Sandia National Laboratories). This work was performed under the auspices of the U.S. Department of Energy, Office of Vehicle Technologies, Hybrid and Electric Systems, under Contract Nos. DE-AC02-06CH11357 (ANL) and DE-AC07-99ID13727 (INL).

References

[1] FY2008 Progress Report for Energy Storage Research and Development, U.S. Department of Energy, January 2009. http://www1.eere.energy.gov/vehiclesandfuels/pdfs/program/2008_energy_storage.pdf.
[2] L. Wang, J. Li, X. He, W. Pu, C. Wan, C. Jiang, J. Solid State Electrochem. 13 (2009) 1157–1164.
[3] D.J. Jang, Y.J. Shin, S.M. Oh, J. Electrochem. Soc. 143 (1996) 2204–2211.
[4] K.W. Nam, W.S. Yoon, H. Shin, K.Y. Chung, S. Choi, X.Q. Yang, J. Power Sources 192 (2009) 652–659.
[5] Y. Xia, Y. Zhou, M. Yoshio, J. Electrochem. Soc. 144 (1997) 2593–2600.
[6] Y. Xia, M. Yoshio, J. Power Sources 66 (1997) 129–133.
[7] R.J. Gummow, A. de Kock, M.M. Thackeray, Solid State Ionics 69 (1994) 59–67.
[8] J. Vetter, P. Novák, M.R. Wagner, C. Veit, K.-C. Möller, J.O. Besenhard, M. Winter, M. Wohlfahrt-Mehrens, C. Vogler, A. Hammouche, J. Power Sources 147 (2005) 269–281.
[9] J. Fergus, J. Power Sources 195 (2010) 939–954.
[10] S.K. Jeong, J.S. Shin, K.S. Nahm, T.P. Kumar, A.M. Stephan, Mater. Chem. Phys. 111 (2008) 213–217.
[11] A. Manthiram, W. Choi, J. Electrochem. Soc. 10 (2007) A228–A231.
[12] J. Goa, A. Manthiram, J. Power Sources 191 (2009) 644–647.
[13] I. Bloom, B.W. Cole, J.J. Sohn, S.A. Jones, E.G. Polzin, V.S. Battaglia, G.L. Henriksen, C. Motloch, R. Richardson, T. Unkelhaeuser, H.L. Case, J. Power Sources 101 (23) (2001) 8–247.
[14] R.B. Wright, C.G. Motloch, J.R. Belt, J.P. Christophersen, C.D. Ho, R.A. Richardson, I. Bloom, S.A. Jones, V.S. Battaglia, G.L. Henriksen, T. Unkelhaeuser, D. Ingersoll, H.L. Case, S.A. Rogers, R.A. Sutula, J. Power Sources 110 (2002) 445–470.
[15] I. Bloom, S.A. Jones, V.S. Battaglia, G.L. Henriksen, J.P. Christophersen, R.B. Wright, C.D. Ho, J.R. Belt, C.G. Motloch, J. Power Sources 12 (2003), 538.
[16] I. Bloom, A.N. Jansen, D.P. Abraham, J. Knuth, S.A. Jones, V.S. Battaglia, G.L. Henriksen, J. Power Sources 13 (2005), 295.
[17] I. Bloom, B.G. Potter, C.S. Johnson, K.L. Gering, J.P. Christophersen, J. Power Sources 15 (2006), 415.
[18] I. Bloom, L.K. Walker, J.K. Basco, D.P. Abraham, J.P. Christophersen, C.D. Ho, J. Power Sources 195 (2010) 877–882.
[19] Battery Test Manual for Plug-In Electric Vehicles, Rev. 2, INL/EXT-07-12536, December 2010.
[20] Freedom CAR Battery Test Manual for Power-Assist Hybrid Electric Vehicles, DOE/ID-11069, October 2003.
[21] Electrical Vehicle Battery Test Procedures Manual, Rev. 2, January 1996.
[22] Battery Life Estimation software is available at the Argonne Software Shop (http://www.anl.gov/techtransfer/Software_Shop).
[23] (a) E.V. Thomas, I. Bloom, J.P. Christophersen, V.S. Battaglia, J. Power Sources 184 (2008) 312–317;
(b) D. Marquardt, SIAM J. Appl. Math 11 (1999) 431–441;
(c) Data Analysis and Regression, Addison-Wesley, Mosteller and Tukey, 1977;
P.W. Holland, R.E. Welsch, Communications in Statistics: Theory and Methods A6 (1977) 813–827;
B. Iglewicz, in: D.C. Hoaglin, F. Mosteller, J.W. Tukey (Eds.), Understanding Robust and Exploratory Data Analysis, Wiley, New York, 1983, p. 417.
[24] M. Broussely, S. Herreyre, P. Biensan, P. Kasztejna, K. Nechev, R.J. Staniewicz, J. Power Sources 97–98 (1) (2001) 3–21.
[25] G. Smith, Tests and Standards, ASTM International, 2005, pp. 194–197.
[26] J.R. Davis, Heat-Resistant Materials, ASM International, 1997, p. 31ff.
[27] E. Strauss, D. Golodnitsky, E. Peled, Electrochemical and Solid State Letters 2 (1999) 115–117.
[28] G. Blomgren, J. Power Sources 81–82 (1999) 112–118.